Available online at www.sciencedirect.com
SCIENCE DIRECT®
Deep-Sea Research I 52 (2005) 959–978
DEEP-SEA RESEARCH PART I
www.elsevier.com/locate/dsr

Circulation and melting under the Ross Ice Shelf: estimates from evolving CFC, salinity and temperature fields in the Ross Sea

William M. Smethie Jr.*, Stanley S. Jacobs

Lamont-Doherty Earth Observatory of Columbia University, Palisades, NY 10964, USA

Received 14 October 2003; received in revised form 23 July 2004; accepted 19 November 2004
Available online 7 April 2005

Abstract

Temperature, salinity and chlorofluorocarbons (CFCs) 11, 12 and 113 were measured on a line of stations along the front of the Ross Ice Shelf in the austral summers of 1984, 1994 and 2000. Water mass distributions were similar each year but with high variability in the cross-sectional areas. CFC concentrations increased and salinity decreased with time throughout the water column. CFC saturation levels in the shelf and surface waters also increased with time and ranged from 43% to 90%. The undersaturation was due to inflow of low-CFC modified Circumpolar Deep Water, gas exchange limited by sea ice cover and isolation of water from the atmosphere beneath the ice shelf. The residence time of dense shelf waters resulting from sea ice formation is less well constrained by the chemical data than is the strong flow into the Ross Ice Shelf cavity. Shelf waters are transformed over about 3.5 years, by net basal melting of the ice shelf, into fresher Ice Shelf Water (ISW), which emerges as a large plume near the central ice front at temperatures below the sea surface freezing point. We estimate an average ISW production rate of 0.86 Sv and an average net basal melt rate of 60 km^3/year for the Ross Ice Shelf exceeding a 300 m draft (75% of the ice cavity) during recent decades from box and stream tube models fit to all of the CFC and salinity data. Model fits to the individual data sets suggest ISW production and net basal melt rate variability due to interannual changes on a shorter time scale than our observations. ISW production based on the CFC budget is better constrained than net basal melting based on thermohaline data, with a heat budget yielding a rate of only 20 km^3/yr. Reconciling differences between apparent freshwater and temperature changes under the ice shelf involves considerations of mixing, freezing and the flow of meltwater across the ice shelf grounding line.

Keywords: Ice shelf; Circulation; Melting; CFCs; Salinity; Temperature

*Corresponding author. Tel.: +1 845 365 8566; fax: +1 845 365 8155.
E-mail address: bsmeth@ldeo.columbia.edu (W.M. Smethie Jr.).

0967-0637/$ - see front matter © 2005 Elsevier Ltd. All rights reserved.
doi:10.1016/j.dsr.2004.11.016

1. Introduction

The present-day mass imbalance of the Antarctic Ice Sheet is believed to be small, contributing little to global sea-level rise (Church et al., 2001). How that will change in a warmer future climate is a problem of considerable societal relevance. More than 10% of the current ice sheet area floats in the sea, mostly in the form of large, thick ice shelves. These ice shelves are nourished by continental ice that flows across their grounding lines and by precipitation and basal freezing. They lose mass by iceberg calving, surface ablation and bottom melting, the latter comprising a substantial fraction of the annual ice sheet budget (Jacobs et al., 1992; Hellmer, 2004). Basal melting and freezing modifies deep and shelf waters, the dimensions of ice shelves and the rates of sea ice formation. Thus the evolving temperature and salinity of the Southern Ocean (Robertson et al., 2002; Jacobs et al., 2002) have implications for ice shelf melting rates, ice sheet evolution and deep ocean ventilation.

Understanding the basal exchange processes beneath ice shelves has been limited by the difficulty of making direct measurements in the sub-ice cavities, and in fully instrumenting the cavity openings. Knowledge of the sub-ice circulation has been gained from direct measurements of ocean temperature, salinity and currents at a small number of sites (e.g., Zotikov et al., 1980; Nicholls and Makinson, 1998), from numerical models (reviewed by Williams et al., 1998) and from geochemical measurements north of the ice (Weiss et al., 1979; Schlosser et al., 1990; Trumbore et al., 1991; Hohmann et al., 2002). The basal melt/freeze regime has also been inferred from satellite and other observations (Grosfeld et al., 1998; Fricker et al., 2001; Joughin and Padman, 2003). Here we use repeat chlorofluorocarbon (CFC) measurements in the Ross Sea, in combination with wind products and sea ice time series, to calculate time-integrated CFC uptake from the atmosphere. The resulting surface water CFC concentrations and discrete salinity measurements over four decades are then utilized to model the production of Shelf Water, its residence time beneath the Ross Ice Shelf and the net basal melting that transforms it into Ice Shelf Water.

2. Background

Trumbore et al. (1991) used CFC measurements taken in early 1984 to investigate circulation and mixing on the Ross Sea continental shelf and slope, obtaining results consistent with variable ventilation and renewal rates, and with new bottom water formation. Modeling shelf water evolution via gas exchange with the atmosphere, seasonal mixed layer entrainment, and the introduction of external source waters, they estimated shelf water residence times ranging from 2.5 to 4 years. Here we update portions of that study, adding repeat summer 1994 and 2000 salinity and CFC sections to the 1984 transect along the front of the Ross Ice Shelf, revising prior estimates of the surface forcing and sea ice cover and employing a multidecadal record of regional salinity change (Jacobs and Giulivi, 1998; Jacobs et al., 2002). While the basic ocean structure and circulation on the shelf remain essentially as described in Jacobs et al. (1985), water mass properties have evolved over time, most notably a four-decade salinity decrease of $\sim$0.003/yr.

Shelf water formed during winter as a byproduct of intense sea ice production and export (Fig. 1) is more concentrated on the western continental shelf, where sea ice formation is enhanced in persistent coastal leads and polynyas (Killworth, 1974; Kurtz and Bromwich, 1985; Zwally et al., 1985). This produces an east-to-west gradient from Low to High Salinity Shelf Water (LSSW and HSSW), both close to the sea surface freezing temperature. At their northern limit, shelf waters mix with circumpolar deep water (CDW) over the continental slope to form bottom water, and to the south they descend beneath the Ross Ice Shelf, where depression of the freezing point with increased pressure allows the melting of basal ice. This lowers the shelf water temperature and salinity, increasing its buoyancy and causing it to rise along the ice shelf base. Melting is followed by freezing once the in situ freezing temperature is regained, and the resulting Ice Shelf Water (ISW) separates from the basal ice and flows northward out of the ice shelf cavity (MacAyeal, 1985). The feedstocks for shelf waters are surface and intermediate depth flows onto the continental shelf and

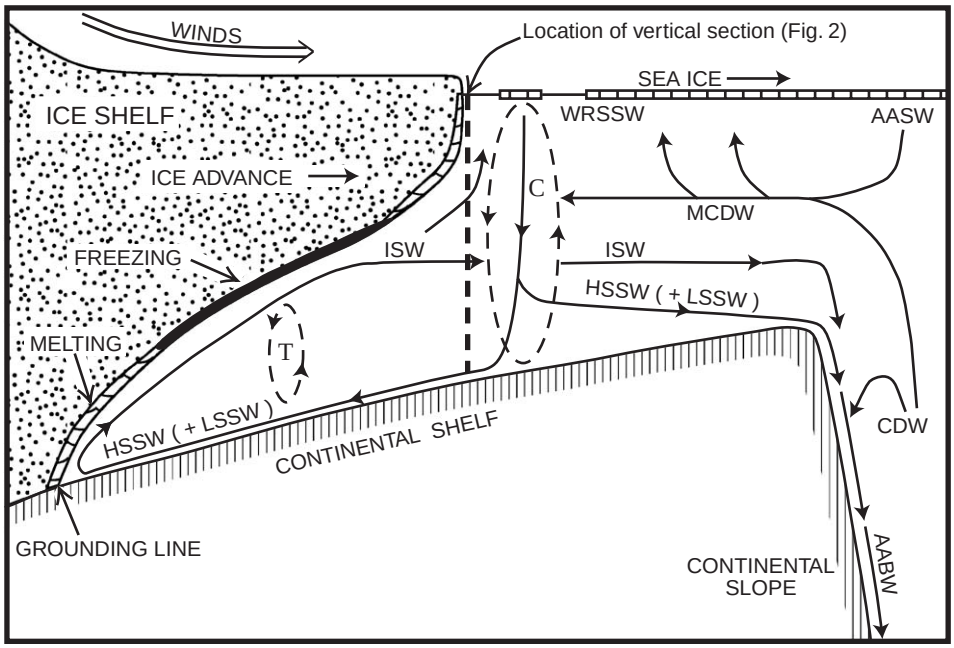

Fig. 1. Schematic diagram of circulation and water mass formation in a vertical plane perpendicular to the Ross Ice Shelf front. AASW = Antarctic Surface Water, CDW = Circumpolar Deep Water, MCDW = Modified Circumpolar Deep Water, WRSSW = Western Ross Sea Surface Water, ISW = Ice Shelf Water, HSSW = High Salinity Shelf Water, LSSW = Low Salinity Shelf Water, AABW = Antarctic Bottom Water. Winter convective mixing is designated by the dashed circulation cell labeled C and tidal mixing is designated by the dashed circulation cell labeled T.

a surface-mixed layer generated by summer warming and sea ice melting. We parameterize the shelf inflows by defining Modified CDW (MCDW) as a mixture of Antarctic Surface Water (AASW) and CDW. AASW layering and properties depend on season and location, with the summer surface-mixed layer on the southwest Ross Sea continental shelf referred to here as Western Ross Sea Surface Water (WRSSW).

CFCs are man-made compounds that have been entering the atmosphere for the past half-century. Their temporal concentrations are known from industrial production records and atmospheric measurements (Elkins et al., 1993; Cunnold et al., 1997; Walker et al., 2000). Chemically stable, CFCs enter the surface ocean by gas exchange with a global oceanic uptake of ~1% of the total emissions through 1994 (Willey et al., 2004). After describing our methods and presenting observations of temperature, salinity and CFC distributions along the front of the Ross Ice Shelf, we develop a box model to account for the temporal change of HSSW CFC concentrations. That model provides the input for box and stream tube models applied to calculate sub-ice shelf cavity residence times, ISW production and basal melting. We compare our results with earlier estimates and with the findings of 3D numerical models recently employed to depict circulation and melting under the Ross Ice Shelf.

3. Observations

3.1. Methods

Ocean stations located near the Ross Ice Shelf in 1984, 1994 and 2000 are shown in Fig. 2. CTD measurements were made with a Neil Brown Mark III system in 1984 and a Seabird 911 system in 1994 and 2000. Temperature and conductivity sensors were calibrated before and after each

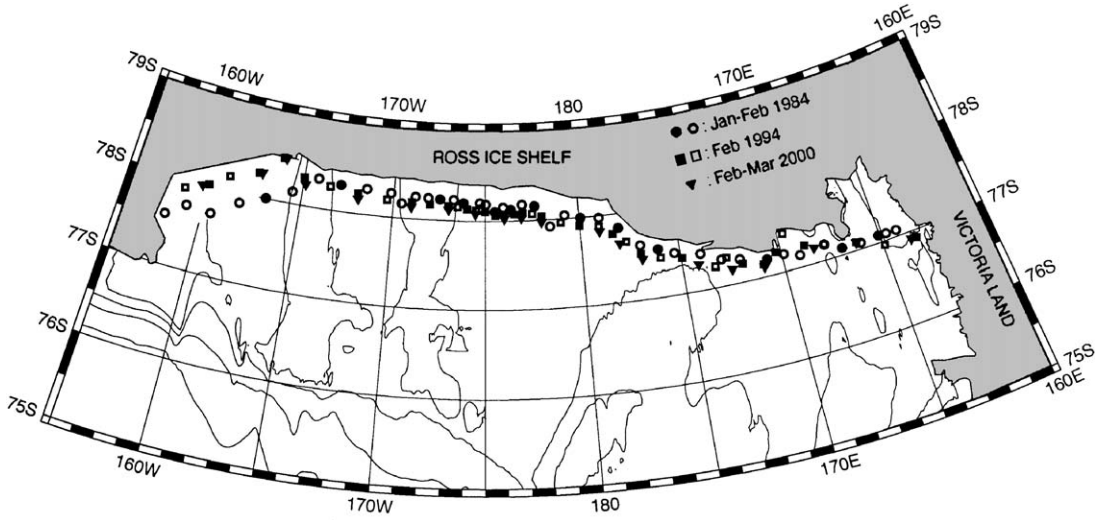

Fig. 2. Station locations (solid symbols, CTD and CFC measurements; open symbols, CTD only measurements) in 1984, 1994, and 2000 near and west of the front of the Ross Ice Shelf. Most stations were occupied within several hundred meters of the ice front, which advances slowly northward, followed by abrupt large-scale calving events.

cruise, and the salinity data further adjusted if necessary to bottle salinity measurements with Guildline Autosals. Water samples were collected using 12- and 24-place rosettes interfaced to the CTD. Five-liter bottles were used in 1984 and 10-l bottles in 1994 and 2000, all fitted with vacuum oven-baked o-rings and epoxy-coated stainless steel springs.

CFC measurements were made with a purge and trap system interfaced to a gas chromatograph equipped with an electron capture detector (Bullister and Weiss, 1988). CFC-11 and CFC-12 were measured on board ship in 1984 (Trumbore et al., 1991). In 1994 and 2000, CFC samples were collected in flame-sealed glass ampoules (Busenberg and Plummer, 1992; Mensch et al., 1998) and analyzed within a few months of collection by a variation of the above method (Smethie et al., 2000) that also includes CFC-113. Measurement precision in 1984 was 0.04 and 0.02 pmol/kg for CFC-11 and CFC 12 and in 1994 and 2000 was the larger of 1% or 0.01 pmol/kg for CFC-11, 2.5% or 0.01 pmol/kg for CFC-12, and 0.03 pmol/kg for CFC-113. All results presented here have been converted to the SIO 93 calibration scale.

3.2. Temperature, salinity and CFC distributions

Vertical sections of potential temperature, salinity, and CFC-12 along the front of the Ross Ice Shelf were prepared by interpolating the observations onto a ~25 km × 25 m grid and computer contouring the resulting array (Fig. 3). CFC-11 and CFC-113 distributions are similar to the CFC-12 sections. HSSW is most clearly seen in the salinity distribution, intensified at the deep western (right) end of the section. The lower salinity LSSW lies mainly along the bottom in the east, and the primary lobe of ISW is clearly delineated at temperatures below −1.92 °C. MCDW is observed as shallower lobes of warmer water above and to the east and (sometimes) west of the ISW, with the eastern lobe typically being more intense and differentiable as two distinct cores on these sections. HSSW and LSSW have the highest CFC concentrations of the four sub-surface water masses. CFC concentrations are lower in ISW, which has been isolated from exchange with the atmosphere beneath the Ross Ice Shelf, and in MCDW, which contains a large component of very low CFC Circumpolar Deep Water. The basic

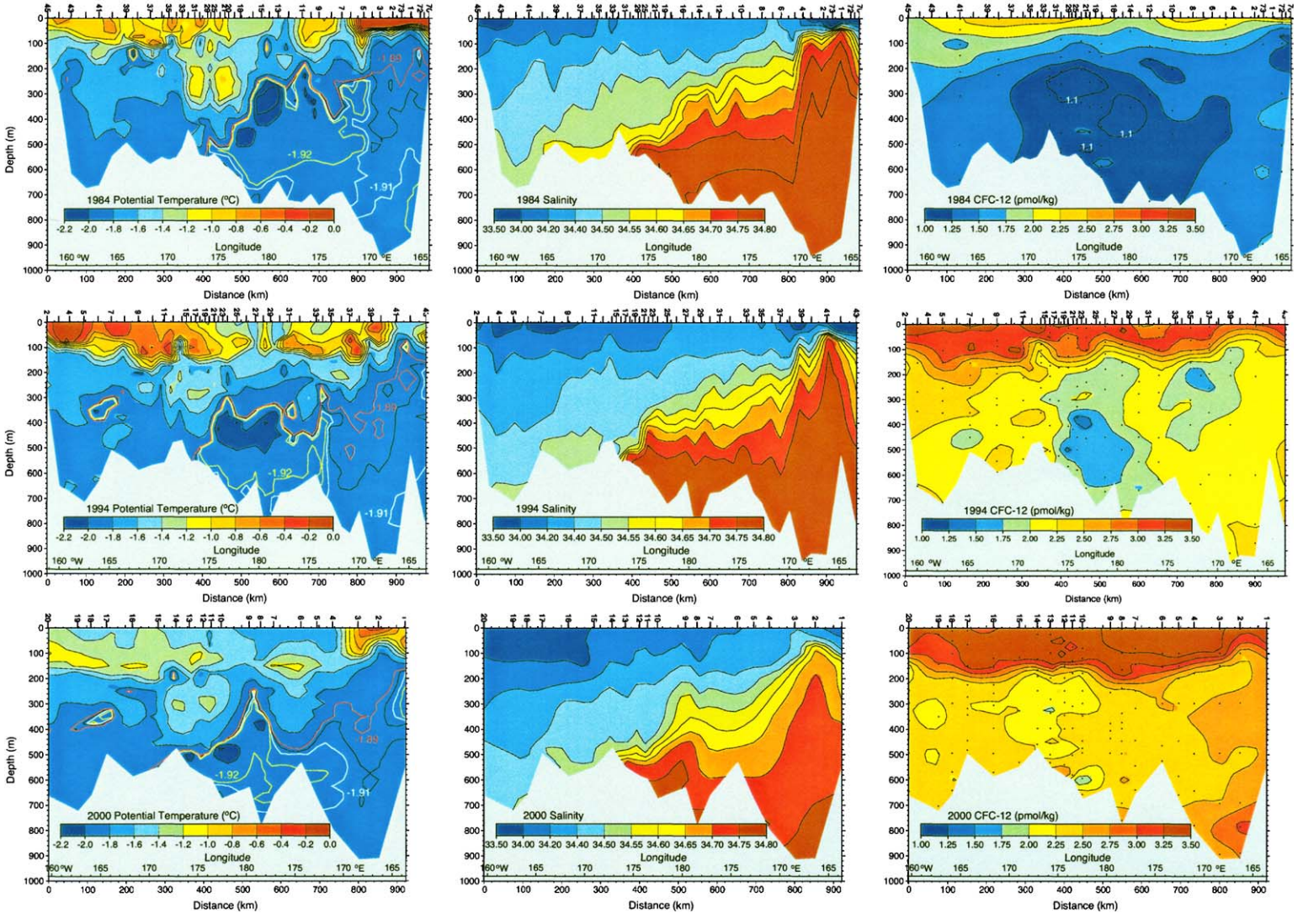

Fig. 3. Vertical sections of CTD potential temperature and salinity and discrete CFC-12 measurements along the front of the Ross Ice Shelf in 1984, 1994, and 2000. The views are southward, looking into the sub-ice cavity (Fig. 1) and result from contoured gridded data taken at the stations shown along the top of each panel and in Fig. 2. The colored potential temperature isolines are as follows: red = −1.89 °C, white = −1.91 °C, yellow = −1.92 °C.

structure of the sections is the same each year, with the freshening over time complemented by increasing CFC levels, due to rising atmospheric concentrations. Rapid ventilation of all water masses (Trumbore et al., 1991) is graphically confirmed by the increasing CFC-12 concentrations since 1984 (Fig. 3).

4. Results

4.1. Average potential temperature, salinity and CFC concentrations for WRSSW, HSSW and ISW

The core regions of HSSW and ISW in the vertical sections were defined by depth and thermal properties after examining data from the three cruises reported here as well as earlier sections along the Ross Ice Shelf (Jacobs and Giulivi, 1998). HSSW was required to have a potential temperature between –1.91 and –1.89 °C, bracketing the surface freezing temperature, and to be located west of 180° and below 300 m. Waters with potential temperature below –1.92 °C, deeper than 180 m and west of 173°W were considered to be part of the primary ISW outflow from beneath the ice shelf. WRSSW was defined as occupying the upper 50 m west of 172°E. Mean values (Table 1) were obtained by averaging over all grid points bounded by the defined temperature, depth and location. While all sections were occupied during the same time of year (22 January–17 February), surface water property variability resulted from short-term changes in atmospheric forcing and high near-surface gradients. HSSW and ISW cross-sectional areas along the ice shelf front are also variable, resulting in part from definitions employed for these water masses. We discuss the ISW variability in more detail below.

4.2. High Salinity Shelf Water model

We use a time-dependent box model similar to that of Trumbore et al. (1991) to gain insight into HSSW formation and to obtain temporal CFC concentrations as boundary conditions for ISW production. CFCs can enter HSSW directly from

Table 1
Average values of potential temperature, salinity, CFC-11, CFC-12, CFC-113 and the cross-sectional areas along the Ross Ice Shelf for WRSSW, HSSW and ISW and percent saturation for WRSSW and HSSW

Date	Water mass	Potential Temp (°C)	Salinity	CFC-11 (pmol/kg)	CFC-11 % saturation	CFC-12 (pmol/kg)	CFC-12 % saturation	CFC-113 (pmol/kg)	CFC-113 % saturation	Area (km^2)
22 Jan–2	WRSSW	–0.257	34.198	3.61	64	2.00	79			22
Feb 1984	HSSW	–1.904	34.820	2.53	44	1.43	56			62
	ISW	–1.968	34.719	2.32		1.19				91
6 Feb–10	WRSSW	–1.106	34.115	5.78	74	2.90	79	0.54	69	22
Feb 1994	HSSW	–1.902	34.765	4.42	56	2.15	58	0.35	43	115
	ISW	–1.975	34.710	3.71		1.80		0.24		68
15 Feb–17	WRSSW	–0.996	34.310	6.51	84	3.48	90	0.61	75	17
Feb 2000	HSSW	–1.901	34.727	5.01	65	2.59	67	0.45	56	97
	ISW	–1.957	34.686	4.74		2.34		0.39		42

the atmosphere by gas exchange, indirectly after uptake by WRSSW, and by mixing with the AASW/CDW composite (MCDW) that flows onto the shelf (Fig. 4). During summer (Dec–Mar), the ice cover is usually low and a surface-mixed layer can be differentiated from the deeper waters by density stratification. From a late summer-mixed layer thickness of ~90 m in 1984, we assume that WRSSW entrains underlying HSSW as it deepens from 22.5 to 90 m from December through March. If most MCDW flows onto the shelf from the northeast, AASW can be represented by a region bounded by 73.0–77.5°S, 130–160°W. There a winter-mixed layer of AASW extends to about 200 m beneath a 20 m mixed layer during late summer (Jacobs et al., 2002). Analogous to WRSSW on the shelf, then, an early summer 5 m surface-mixed layer is increased linearly to 20 m by the end of summer.

By April sea ice covers the continental shelf, and brine rejection is raising the density of the surface layer. WRSSW mixing into the underlying HSSW strengthens during winter with HSSW eventually extending from surface to bottom on portions of the western continental shelf. HSSW production and CFC uptake from the atmosphere are more concentrated in open polynyas near the ice shelf and along the Victoria Land coast, from where the dense water sinks and spreads laterally to the interior. Since HSSW probably does not occupy the entire 515 m of the water column during all winter months, one set of simulations assumed a mean thickness of 400 m, to investigate the model sensitivity to this parameter.

Flow of MCDW onto the continental shelf is assumed to occur year round at a constant rate, balanced by water flowing off the shelf. Trumbore et al. (1991) parameterized the MCDW as a 40:60 ratio of AASW:CDW based on a θ/S analysis of the 1984 data set. We ran four simulations using fixed ratios of 40:60, 45:55, 50:50, and a variable ratio increasing from 36:64 in 1960 to 42:58 in 2000 to reflect the temporal decrease in shelf water salinity. The CFC concentration in CDW was ~2.5% of saturation for CFC-11 and CFC-12 and 1.5% of saturation for CFC-113 in 2000. The CFC concentration as a function of time in CDW is assumed to track the atmospheric concentrations at these very low saturations but this has little influence on the model calculations.

The model was run with a time step of 0.1 month and a wind-dependent gas exchange coefficient from Wanninkhof (1992):

$$K = 0.39\ U^2(Sc/660)^{-0.5},$$

where K is the gas exchange coefficient, U is the monthly average wind speed and Sc is the Schmidt number of the gas. The values of Sc for CFC-11, CFC-12 and CFC-113 at –1.8 °C are respectively 4544, 4176 (Wanninkhof, 1992), and 5653 (Wanninkhof, personal communication). We assumed the surface water to remain at the freezing point year round because of the presence of sea ice and thus the Schmidt numbers are constant. Monthly values for wind speed (averages of instantaneous wind speeds) and sea ice concentration were averaged from NCEP (2002), post-1978, and from Jacobs and Comiso (1989) and NSIDC

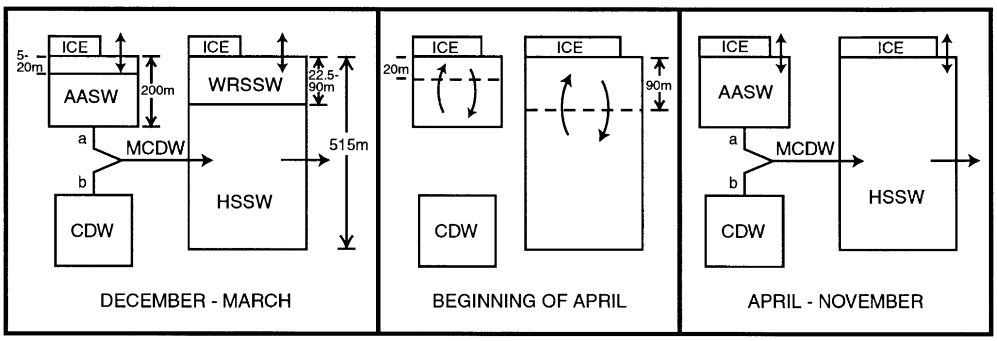

Fig. 4. Schematic diagram of the HSSW box model through an annual cycle. See Fig. 1 for water mass labels. The mean depth of the western shelf is taken to be 515 m, averaged from Davey (1995).

(http://nsidc.org). Speeds ranged from 4(6) to 7(8) m/s and ice cover averaged 11(95)% in summer(winter) months (Table 2). Both winds and summer ice concentrations were lower on the continental shelf, with better support for the latter than the former. Atmospheric CFC concentrations were taken from Walker et al. (2000).

The CFC observations were fit equally well with different sets of parameters, with a lesser HSSW thickness requiring a greater input of MCDW. Increasing the ratio of AASW:CDW in MCDW also required more MCDW, from a water column replacement of 80 m/yr for a 40:60 mixture to 140 m/yr for a 50:50 mixture. Three best-fit simulations of the HSSW CFC concentrations and the HSSW and WRSSW CFC averages from Table 1 are presented in Fig. 5 and Table 3. HSSW residence time is clearly sensitive to its mean thickness and inflow characteristics, neither of which are well defined by these data sets. While the ranges in Table 3 are reasonable bounds for these parameters, they do not effectively constrain HSSW residence time. Nonetheless, any of the HSSW simulations can provide the evolving CFC concentrations needed for Ice Shelf Water models, which in turn yield additional insight into residence time. As a check on the importance of winter gas exchange, a simulation with 100% ice cover caused a ~20% reduction in HSSW CFC concentration, giving a threshold on the role of winter leads and polynyas on HSSW ventilation and an indication of model sensitivity to ice cover.

4.3. Ice Shelf Water models

The objective of the ISW models is to determine the rate of conversion of HSSW into ISW and the net ice shelf basal melt rate that drives this transformation. We assume that melting and freezing does not appreciably alter the seawater CFC content, and that annual mean inflow and outflow can be characterized by the observed late summer HSSW and ISW properties (Table 1). We focus on what is believed to be the primary circulation cell beneath the ice shelf, i.e., the inflow of HSSW along its western side, and outflow of ISW from the central region (Fig. 3; Jacobs et al., 1992; Holland et al., 2003). Two approaches were used, one assuming that water in the sub-ice cavity is a well-mixed reservoir and the other assuming a stream tube of inflowing HSSW and outflowing ISW (MacAyeal, 1985).

In the reservoir (1-box) model, HSSW inflow mixes rapidly with ambient water and ice shelf meltwater, then outflows as ISW (Fig. 6a). This is represented by

$$dC_{ISW}/dt = [TC_{HSSW} - (T + M)C_{ISW}]/V, \qquad (1)$$

Table 2
Seasonal and monthly average wind speeds since 1978 from NCEP (2002)

Month	Western Cont'l Shelf Wind Speed (m/s)	Western Cont'l Shelf Ice Cover (%)	NE Ross Sea Wind Speed (m/s)	NE Ross Sea Ice Cover (%)
January	4	15	5.1	67
February	4	11	6.6	58
March	4	40	7.5	78
April	7	90	7.9	90
May	7	93	8.4	91
June	7	92	8.6	91
July	7	95	8.2	92
August	7	92	7.7	92
September	7	92	7.4	92
October	7	92	7.4	92
November	7	93	6.0	90
December	4	50	5.2	81

Sea ice concentration for the western continental shelf modified from Jacobs and Comiso (1989), and for the NE Ross Sea from NSIDC files (http://nsidc.org).

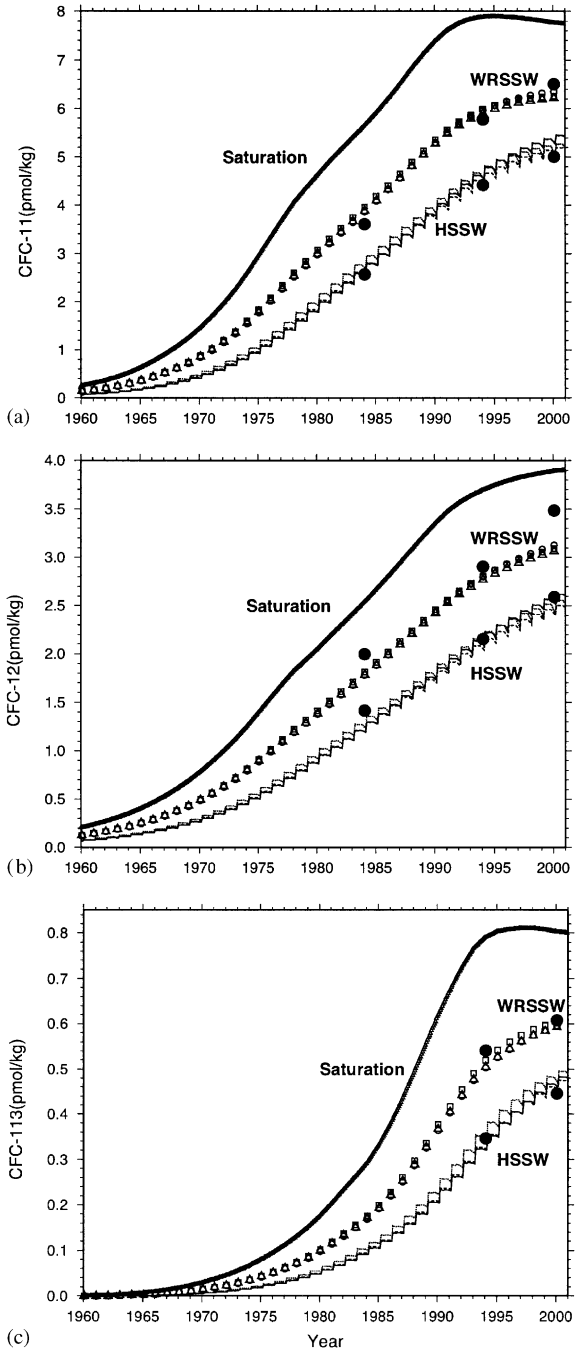

Fig. 5. CFC concentrations vs. time for theoretical open water equilibrium saturation and model simulations of HSSW and WRSSW. Large closed circles represent observations (Table 1). Lines represent simulated HSSW CFC concentrations and symbols WRSSW CFC concentrations in February. Sequential simulations in Table 3 are denoted by square/dotted line, circle/solid line and triangle/dashed line. (a) CFC-11, (b) CFC-12 and (c) CFC-113.

Table 3
HSSW renewal rate as a function of thickness and inflow properties

HSSW thickness	Ratio of AASW:CDW in MCDW	Input of MCDW to the western Ross Shelf	Residence time of HSSW
400 m	36:64–42:58	110 m/yr	3.6 yr
515 m	36:64–42:58	65 m/yr	7.9 yr
515 m	45:55	120 m/yr	4.3 yr

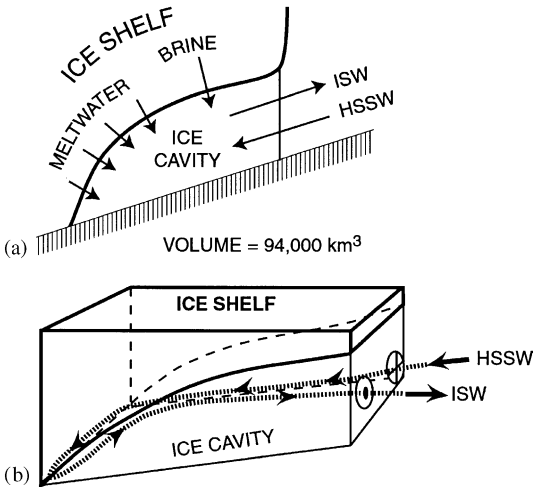

Fig. 6. Schematic diagrams of (a) ISW box model and (b) ISW stream tube model.

where C represents CFC concentration or salinity, T is HSSW volume transport into the reservoir, M is meltwater input, V is reservoir volume, and t is time. V is assumed to be constant with net basal melting balanced by glacier flow from the continent. Since meltwater lacks CFCs and $M < 0.3\%$ T, Eq. (1) can be rewritten for CFCs as

$$\begin{aligned} dC_{ISW}/dt &= (T/V)(C_{HSSW} - C_{ISW}) \\ &= (1/t_R)(C_{HSSW} - C_{ISW}), \end{aligned} \quad (2)$$

where t_R is the residence time. With ice shelf and water column thickness and ice shelf area from Bentley et al. (1979), Greishar and Bentley (1980) and Fox and Cooper (1994), the applicable

reservoir volume is ~94,000 km^3, estimated for the inner cavity where the ice draft exceeds ~300 m. This accounts for three-fourths of the total ice cavity volume.

Eq. (2) was solved numerically for 1940–2001, with the initial CFC concentration at zero and its evolution in HSSW as a function of time taken from the HSSW model (Fig. 5). Varying cavity residence time to obtain fits to the average ISW CFC concentrations (Table 1), gave a range of 0.9–5.4 years (Fig. 7), corresponding to volume transports of 3.3–0.55 Sv. The wide range reflects both noise in the method of calculation and natural variability, with a residence time of 3.4 years and corresponding transport of 0.88 Sv providing the best overall fit.

Eq. (1) was then solved numerically for salinity for the 1960–2001 time period and $T = 0.88$ Sv. The salinity of inflowing HSSW as a function of time was taken from a trend based on observations at 500 m near the western end of the Ross Ice Shelf (Jacobs et al., 2002) consistent with changes at that depth over the western shelf (Jacobs and Giulivi, 1998) and with the HSSW averages in Table 1 (Fig. 8). An average 1976 ISW salinity of 34.768 was calculated from earlier data and an initial (1960) ISW salinity of 34.816 was obtained by extrapolating a linear regression through the 1976–2000 observations, which parallel the contemporary HSSW salinity trend. For a cavity residence time of 3.4 years, net freshwater additions could have ranged from ~46 to 70 km^3/yr between 1960 and 2000 (Fig. 8). Volume transports of ISW outflows and basal melt rates associated with the residence times for individual CFC observations are summarized in Table 4. The average residence time based on individual data sets increases dramatically from 1984 to 1994 and weighting 1984, 1994 and 2000 equally yields an overall average melt rate of 77 km^3/yr. For a constant residence time of 3.4 years, the overall melt rate that best fits the ISW salinity data from 1976 to 2000 is 57 km^3/yr (Fig. 8). We believe the 1984 result is caused by short-term variability and that 57 km^3/yr is the best estimate for the overall average melt rate (see Discussion).

In the stream tube model, HSSW enters the cavity near the sea floor and flows along the

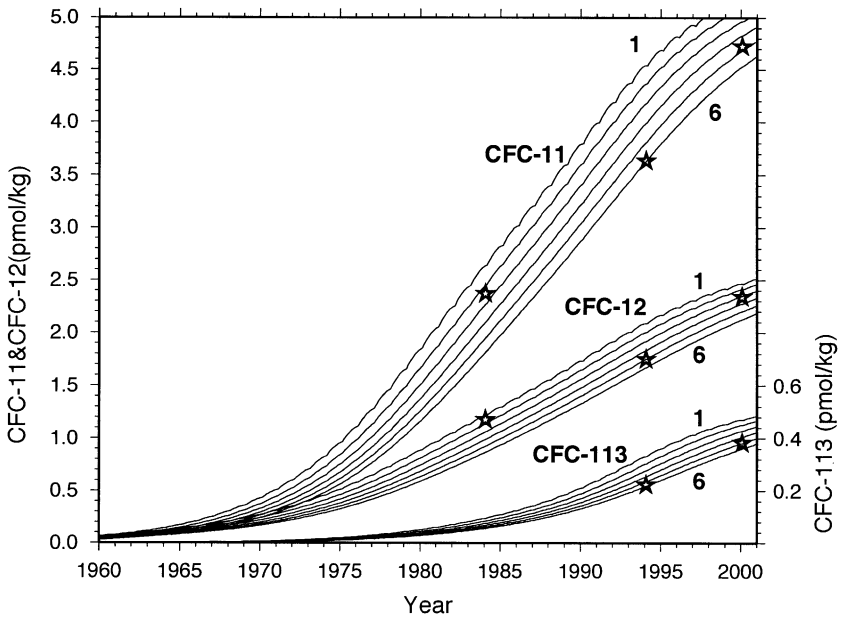

Fig. 7. Observed (stars) and modeled (solid lines) CFC concentrations in ISW vs. time. Model concentrations were calculated using the ISW box model (Eq. (2), Fig. 6a) for residence times of 1–6 years.

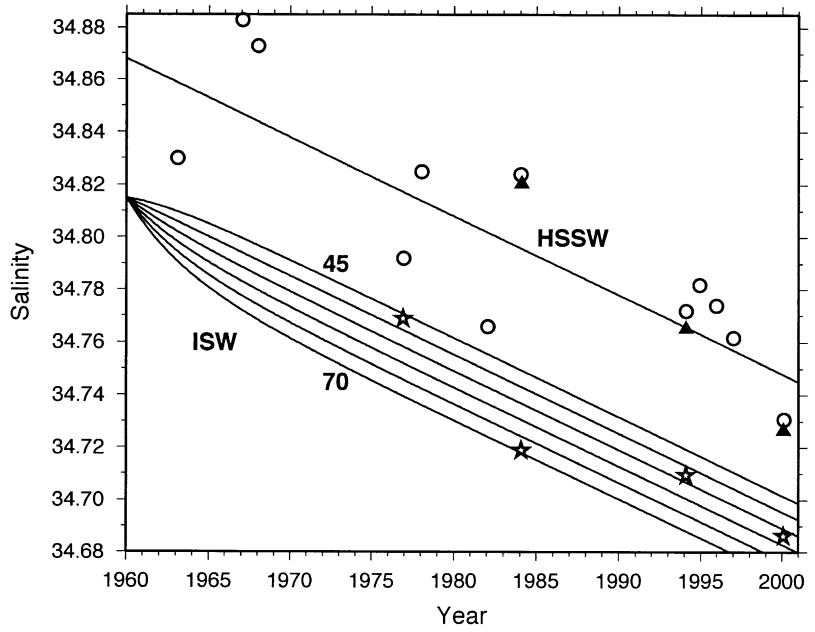

Fig. 8. HSSW salinity vs. time from Jacobs et al. (2002) (open circles) and from this study (Table 1; solid triangles), with the single upper line a linear regression fit to the open circles. The Jacobs et al. (2002) data are from 500 m depth at a location near the western end of the Ice Shelf front (see their Fig. 3a). ISW salinity from this study (Table 1; stars) and from the ISW box model (Eq. (1), lower lines) with a residence time of 3.4 years and melt rates ranging from 45 to 70 km^3/yr.

Table 4
Residence times, transit times, current speeds, ISW volume transports, and basal melt rates calculated from the ISW box and stream tube models and the CFC and salinity observations

Year	CFC	Residence time (yr) Box model	Transit time (yr) Stream tube	Current speed (cm/s) Stream tube	ISW volume transport (Sv) Box model (Stream tube)	Melt rate (km^3 water/yr) Box model (Stream tube)
1984	11	1.6	2.5	1.9	1.86 (1.27)	132 (97)
	12	0.9	1.0	4.8	3.32 (3.18)	180 (228)
1994	11	5.4	5.5	0.9	0.55 (0.58)	29 (39)
	12	4.6	4.5	1.1	0.65 (0.71)	34 (45)
	113	4.5	4.0	1.2	0.66 (0.80)	35 (50)
2000	11	5.0	6.5	0.7	0.60 (0.49)	36 (36)
	12	3.4	4.0	1.2	0.88 (0.80)	50 (53)
	113	4.0	4.5	1.1	0.75 (0.71)	44 (49)

grounding line where it is modified by basal melting. This causes it to become fresher and colder, and the lighter return flow exits the cavity near the center of the ice front (Fig. 6b). The addition of meltwater again has a negligible effect on CFC concentration, but here it is assumed that no mixing occurs between the HSSW/ISW stream tube and the ambient environment. The CFC concentration of ISW arriving at the ice front is thus the same as inflowing HSSW at some earlier point in time, which can be read off the CFC time history for HSSW (Fig. 5), in turn providing the

transit time. Volume transport is then equal to transit distance, ~1500 km, divided by transit time and multiplied by the cross-sectional area of ISW outflow near the ice front. Because ISW cross-sectional areas suggest temporal variability, we use the average area of our observations in Table 1, 67 km^2. Melt rate is then calculated from

$$M = [(S_{inflow} - S_{outflow})/S_{inflow}]T, \quad (3)$$

where salinity (S) of the inflowing HSSW was taken from the upper trend in Fig. 8 and the average ISW outflow salinity from Table 1. Transit time through the ice cavity is about 2 years for 1984, and 5 years for 1994 and 2000 with an overall average of about 3.8 years corresponding to an ISW transport out of the ice cavity of 0.84 Sv (Table 4). Weighting each year equally, the melt rate would be 84 km^3/yr but using the constant 3.8 year transit time and 0.84 Sv ISW transport yields 60 km^3/yr, which is probably a better estimate for the overall average.

5. Discussion

5.1. Variability

The data presented in this study have been interpreted to yield average water mass residence times, transports and net basal melt rate for the deeper portions of the Ross Ice Shelf over roughly three decades. However, there is clearly strong variability on shorter time scales, apparent in the scatter of HSSW salinity about the decreasing trend since 1960. For example, the difference in the HSSW salinity between 1982 and 1984 is 0.06, half the difference in the trend between 1960 and 2000 of 0.12 (Fig. 8). However, the scatter about the salinity trend for ISW is less, and the nearly parallel trends of HSSW and ISW salinities suggest that interannual variability tends to be smoothed over the time scale of regional circulation.

Variability is also apparent in our three data sets. The cross-sectional area of ISW and HSSW along the front of the Ross Ice Shelf varies by a factor of two, but not in concert (Table 1). Some of this variability reflects changes in surface forcing and in the sources and sinks for the larger HSSW reservoir. Variability over the shelf region can also reach into the sub-ice cavities, as evidenced by direct observations and numerical models (e.g., Hellmer and Jacobs, 1995; Holland et al., 2003; Nicholls and Makinson, 1998; Timmermann et al., 2002b). The box model calculations using our three data sets suggest a factor of 3–4 increase/decrease in the Ross Ice cavity water residence time-transit time/net basal melt rate between 1984 and 1994 (Table 4). NCEP monthly averaged winds from 1970 to 2003 for the western Ross Sea did not show a discernable change between 1984 and later years. One explanation consistent with the data, assuming the 1984 data represents a short transient feature, is described below.

HSSW salinity in 1982 is about 30% lower than the average trend from 1960 to 2000 and ISW salinity in 1984 is lower than its average trend (Fig. 8). The low ISW salinity in 1984 probably results from a low-salinity HSSW precursor such as that in 1982. Since a lower-salinity (and hence density) HSSW may not penetrate as deeply into the Ross ice cavity, the pathway/volume flushed would be shorter/less, corresponding to a shorter CFC residence time beneath the shelf ice. The CFC residence time for 1984 was about 2 years (Fig. 7) consistent with a low-salinity signal propagating from HSSW to ISW between 1982 and 1984. The apparent high net basal melt rate for 1984 results from the short residence time, which yields a larger transport that is multiplied by the salinity difference between HSSW and ISW. Being less dense than normal, the 1984 ISW should exit the ice shelf cavity higher in the water column than vintages formed from denser HSSW. The bulk of water colder than −2 °C is indeed about 100 m shallower in 1984 than in 1994 or 2000 (Fig. 3). Such a mechanism demonstrates how interannual variability in ice cavity flushing and apparent basal melt rates could be generated by HSSW salinity variability. Because the temporal data coverage needed to address interannual variability are lacking and local circulation appears to smooth out this variability, we have focused on model results that best fit the aggregate data set, representing multidecadal means of ice cavity flushing and basal melt rates.

5.2. Shelf water CFC saturations

The continental shelf waters around Antarctica are mostly ice covered for most of the year, with significant CFC undersaturations (Trumbore et al., 1991; Orsi et al., 2002). In the surface water of the southwestern Ross Sea in early 1984, 1994 and 2000, CFC concentrations ranged from 64% to 90% saturation. Levels were highest for CFC-12 and lowest for CFC-113, reflecting differences in gas exchange rates and atmospheric time histories, and increased with time for all CFCs (Table 1) as CFC concentrations leveled off in the atmosphere during the 1990s. The HSSW box model includes CFC uptake from the atmosphere, and agrees fairly well with the observed CFC undersaturations (Fig. 5), which can be explained as follows: First, the WRSSW remains well below saturation during summer in spite of exposure to the atmosphere because of progressive entrainment of underlying HSSW, MCDW and possibly ISW as the wind-mixed surface layer deepens. Second, the MCDW that is entrained year-round has a large CDW component with a very low CFC concentration. Third, gas exchange through the limited open water during winter, and sometimes in summer, is not fast enough to equilibrate the HSSW as it is modified directly by sea ice formation and export. These processes demonstrate the complexity of parameterizing gas exchange and mixing for calculations of uptake of a variety of gases by dense water formed in the polar environment. Furthermore, with shelf water CFC concentrations rising as the atmospheric concentrations are leveling off (Table 1), saturations cannot be assumed to be a constant fraction of 100%, as in Orsi et al. (2002).

5.3. High Salinity Shelf Water

Our estimated residence time of HSSW on the western Ross continental shelf ranges from 3.6 to 7.9 years, with respect to the inflow of MCDW, an average over ~3 decades since 1970, during which about 95% of the CFC input has occurred. Trumbore et al. (1991) estimated a residence time of 4 years for HSSW from the 1984 CFC-12 data. Although we now have a better knowledge of the ice cover, if not wind speed, and increased resolution of the CFC changes from three sets of observations over a 16-yr period, uncertainties in the total volume of HSSW and the composition of MCDW preclude refinements to that earlier estimate. However, the apparently robust 0.86 Sv conversion rate of HSSW to ISW requires a relatively short residence time for HSSW. If HSSW nearly fills the $1.29 \times 10^5\,km^3$ western Ross Sea (Jacobs et al., 1970), then a residence time of 7.9 (3.6) years implies a production rate of 0.52 Sv (1.14 Sv) of which nearly 0.86 Sv must flow into the sub-ice cavity to produce the primary ISW outflow. Given that bottom water also forms directly from HSSW, the transformation of a large fraction into ISW constrains its volume and renewal rate to values corresponding to a residence time near the low end of our range. In the Weddell Sea, Mensch et al. (1996) estimated a 5-yr residence time for Western Shelf Water, equivalent to HSSW in the Ross Sea, based on a box model calculation for tritium and CFC concentrations taken between 1985 and 1987.

5.4. Ice Shelf Water

5.4.1. Production and basal melt rate

The models yielded mean ISW residence and transit times in the cavity of 3.4 and 3.8 years, formation rates of 0.88 and 0.84 Sv, and net basal melt rates of 57 and $60\,km^3/yr$. This assumes that seawater near the front of the Ross Ice Shelf deeper than its draft and colder than the surface freezing point contains a component of meltwater from the underside of the ice shelf. Defined here as having a potential temperature less than –1.92 °C, this ISW often appears to include separate streams of water that may have had different degrees of interaction with the base of the ice shelf and adjacent waters. This ISW definition excludes meltwater that has ended up in water warmer than −1.92 °C, but may include freshwater that has crossed the grounding line. We have also assumed that overall averages and trends are more important than interannual variability, and that the melt rate can be determined from a salt budget. The similar result obtained from the two models is probably fortuitous, given these and other

assumptions, such as transit distance and cavity volume. Volume transport is better constrained in the box model, from which the 57 km^3/yr of meltwater would be equivalent to an average melt rate of ~19 cm/yr over 330,000 km^2 of the ice shelf base. Of course very little of the base will melt at that specific rate, as strong melting near deep grounding lines and the ice front is partially balanced by weak melting or freezing over much of the central ice shelf (Neal, 1979; Zotikov et al., 1980; Rignot and Jacobs, 2002; Assmann et al., 2003; Holland et al., 2003). In addition, the primary circulation cell evaluated here does not address basal melting and freezing under the outer portion of the ice shelf where its draft is less than 300 m, and a salinity vs. temperature budget anomaly remains to be accounted for.

5.4.2. The salinity vs. temperature budget anomaly

Trumbore et al. (1991) noted that different meltwater estimates could be obtained by using the temperature or the salinity change between inflowing HSSW and outflowing ISW and suggested this anomaly might result from ice crystal formation in the water column or lower inflow salinities than observed. Ice crystals have been reported in Weddell Sea ISW (Dieckmann et al., 1986), and could impact the heat and freshwater budgets of ISW. And as discussed earlier, relatively low HSSW salinity in 1982 may explain the low ISW salinity in 1984 (Fig. 8). On the longer term, however, the HSSW salinity was higher 3.4–3.8 years prior to the time it was measured along with ISW salinity.

The heat of fusion required to melt glacial ice and the flux of heat from seawater into the ice require that seawater temperature and salinity decrease in a particular ratio, which can be derived as follows. The apparent melt rate, M, is estimated from the change in salinity between water flowing into and out of an ice cavity, as

$$M = (\Delta S/S_i)T,$$

where ΔS is the change in salinity, S_i is the salinity of inflowing water and T is the volume transport. If melting were the only heat sink, then the melt rate could be calculated from the temperature change between inflow and outflow, as

$$M = (T\Delta\theta H_c)/H_f,$$

where $\Delta\theta$ is the change in potential temperature, H_c is the specific heat capacity of seawater and H_f is the latent heat of melting. Equating these two expressions for M and assuming $H_c = 4 \times 10^3$ J/kg and $H_f = 3.347 \times 10^5$ J/kg yields $\Delta\theta/\Delta S = 84/S_i$. The salinity of HSSW is about 34.8 (Fig. 8) which implies that $\Delta\theta/\Delta S = 2.4$, but the very cold shelf ice ($< -20\,^\circ$C at the upper levels) is another heat sink, estimated to absorb about 10% of the heat required for melting (Jenkins et al., 1997). This alters the $\Delta\theta/\Delta S$ ratio to 2.65, similar to more thorough derivations and to field observations near the ice (Gade, 1979; Nost and Foldvik, 1994; Hellmer et al., 1998; Nicholls et al., 2001).

Temperature and salinity changes during the conversion of HSSW to ISW in the Ross Ice Shelf cavity can be calculated from the temperature averages in Table 1, the decreasing salinity trend for the region (Fig. 8) and the 3.4 year residence time estimated for water in the ice cavity. An average $\Delta\theta/\Delta S$ near 1.0 implies a salinity change more than twice what can be accounted for by the apparent HSSW to ISW heat loss. On a θ/S diagram (Fig. 9), ISW can be related to its presumed HSSW source and to other waters with which it may have mixed. The LSSW average is obtained from depths >500 m east of the ISW core. Solid lines sloping from upper right to lower left indicate the Melt–Freeze (M–F) relation calculated above for glacial ice melting into seawater ($\Delta\theta/\Delta S = 2.65$). The M–F slope nearly connects the LSSW and ISW_{J9}, consistent with a separate circulation cell (e.g., Nost and Foldvik, 1994). ISW_{EX} (the coldest water observed in the ISW plume) is close to the M–F slope through HSSW, but the connection is poor between the mean HSSW inflow and ISW outflow, the latter being too warm for the observed salinity change, or too fresh for the observed temperature change.

There are several ways to account for this anomaly in the $\Delta\theta/\Delta S$ ratio. To the extent that platelet ice forms in and warms the ISW plume (Jenkins and Bombosch, 1995), an imbalance could occur between upward movement of

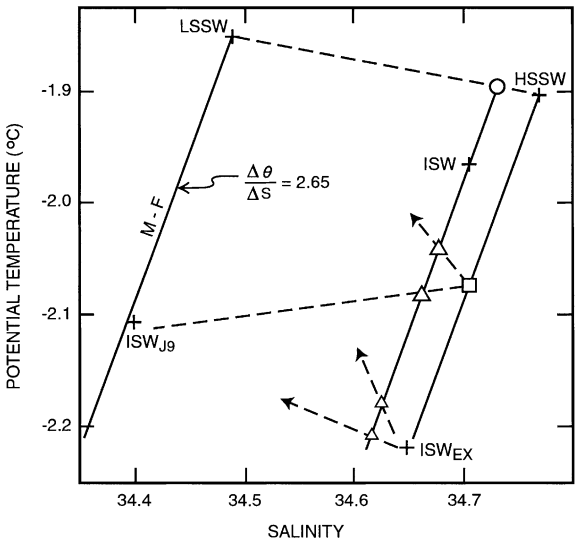

Fig. 9. A potential temperature/salinity diagram illustrating melting, freezing and mixing processes that can lead to formation of the primary Ice Shelf Water (ISW) outflow plume from beneath the Ross Ice Shelf. Observed values (+) are averages for 1984, 1994 and 2000, from Table 1, except ISW_{EX} is the coldest water observed in that plume, and ISW_{J9} the average upper boundary layer (~100 m) properties measured beneath the ice shelf at J-9 (82.38S, 168.62W) in 1977–78 (Jacobs et al., 1979). By melting and freezing (M–F) at the base of the ice shelf, the properties of the boundary layer move along the solid lines, which have $\Delta\theta/\Delta S$ slopes of 2.65. The dashed lines indicate possible mixing between observed varieties of ISW and the high and low-salinity shelf waters (HSSW and LSSW).

freshwater and downward loss of brine. By assuming that most of the heat for melting comes from HSSW and total melting is set by the salinity budget, a colder intermediate ISW type (open square in Fig. 9) could mix with fresher ISW_{J9} or LSSW, generating properties near the large open triangles on the M–F line through ISW. Subsequent upwelling, freezing and warming would restore the observed ISW product. A similar mixing scenario, beginning with ISW_{EX}, could also account for ISW outflow properties, analogous to the inference of Mensch et al. (1996) for the Weddell Sea, but only if followed by major freezing (Fig. 9). An intermediate ISW type may also recirculate within the cavity and mix back into the HSSW, consistent with some model results and with the dominance of ISW characteristics under the Ronne Ice Shelf (Williams et al. 1998; Nicholls et al., 2001). In that case the open square would move toward HSSW on the M–F line, acquiring heat and salt, followed by mixing with LSSW or ISW_{J9}.

The distribution of water masses on Fig. 9 also suggests that the source water that melts the ice and produces ISW is likely to be a mixture of HSSW and LSSW. LSSW has unobstructed access to the inner Ross Ice Shelf cavity at depths >500 m (Fig. 4 in Bentley and Jezek, 1981) and, while lighter than HSSW by ~sigma 0.25, downward mixing could result from strong tidal activity (MacAyeal, 1984, 1985; Padman et al., 2003; Robertson et al., 2003). A 6:1 mixture of HSSW and LSSW in Fig. 9 would place this potential source water near the open circle on the M–F line through the observed ISW. This would restore the $\Delta\theta/\Delta S$ ratio to 2.65, with basal freezing accommodated by average ISW properties in the cavity that are colder and fresher than observed near the ice front. Geothermal heat flux is negligibly small, but freshwater crossing the grounding line into the sub-ice cavity could alter the salinity budget with little impact on temperature. Without other contributions, however, this would require a much larger volume of freshwater from the grounded ice sheet than estimated (Jacobs et al., 1992).

The appropriate combination of these scenarios cannot easily be determined from the thermohaline and CFC data. Double diffusion and diapycnal mixing between newly formed ISW and other water masses seems likely, enhanced by tidal flows interacting with the sea floor and ice shelf base. The existence of basal marine ice reported by previous studies requires that ISW at the ice front be the net product of melting and freezing. If the amount of freezing is small relative to melting (Assmann et al., 2003; Holland et al., 2003) then the involvement of LSSW could explain most of the average observed ISW properties. If the area of the ice shelf base involved in generating the primary ISW plume includes the J-9 site, the involvement of that water or the intermediate to extreme ISW types would require substantial basal freezing. Of course the heat and salt budgets of HSSW inflow and ISW outflow need not balance in θ/S space if the θ/S properties of the ISW plume are altered by mixing with seawater outside

the ice cavity. For example a 100 m × 50 km 'ring' around the 1984 ISW at the ice front had mean θ/S properties of –1.8 °C and 34.61, which would both warm and freshen the outflow.

Basing the net meltwater production rate on the salinity difference between HSSW and ISW observed near the ice shelf front yields 57–60 km^3/yr. This represents an upper limit, to the extent that mixing with LSSW or with freshwater that crosses the grounding line is not included, but only applies to the ice shelf base deeper than 300 m. Converting the temperature difference between HSSW and ISW to a melt rate yields a value of only 20 km^3/yr. This represents a lower limit to the extent that it does not account for frazil ice effects, ignores warmer and shallower outflows generated over portions of the base near the ice front shallower than 300 m, and assumes no mixing with warmer LSSW and HSSW outside the cavity. Oxygen isotope and neon data (Schlosser et al., 2003) may provide alternate, if not tighter constraints on the net basal melt rate.

5.4.3. Comparisons with other investigations

Several prior studies have estimated melting and freezing beneath the Ross Ice Shelf, using a variety of measurements and models. The earliest of these (Jacobs et al., 1979; Pillsbury and Jacobs, 1985) were concerned with the direct role of MCDW, now thought to be minor because of recirculation near the ice front. MacAyeal (1985) modeled the development of ISW plumes from HSSW, finding a strong dependence of melt rate on depth and temperature of the entrained waters. Shabtaie and Bentley (1987) calculated net melting of 12 cm/yr for the region more than 100 km from the ice front, equivalent to ~46 km^3/yr of meltwater. Scheduikat and Olbers (1990), Lingle et al. (1991) and Hellmer and Jacobs (1995) modeled particular locations or transects. Trumbore et al. (1991) and Jacobs et al. (1992) estimated 79 km^3/yr of meltwater were derived from the same portion of the ice shelf as in this study. That value resulted from averaging fewer, more extreme values of HSSW and ISW from the mid-1980s (Fig. 8), not all measured near the ice front, and was accompanied by an ISW outflow of 1.4 Sv, a larger draw on the available volume of HSSW than required by our estimate. More recently, Bergamasco et al. (2002) reported much lower ISW outflows during 1995 and 1996, 0.018–0.032 Sv compared to our average of 0.86 Sv, probably resulting from their mooring location being on the eastern edge of the ISW cores in Fig. 3, along with assumptions of a narrower (25 km) current and a more restrictive ISW temperature range (<-1.95 °C).

In recent years, regional 3D ocean circulation models have been used to investigate circulation and ice shelf melting around Antarctica and there have been two recent studies of circulation in the Ross ice cavity. Holland et al. (2003) used a version of the Miami Isopycnal Coordinate Ocean Model (MICOM) with the Greishar and Bentley (1980) water column thickness distribution. Heat and freshwater fluxes between the ice and seawater were parameterized with a viscous sub-layer model, and forced by a seasonally variable thermohaline field north of the ice shelf. Strongest melting occurred near the ice front and at interior locations of thick ice, and net freezing over much of the central base. Most ISW outflow occurred around the dateline, as we observed, with an annual mean export of 1.6 Sv along the entire ice shelf front, referenced to a slightly warmer temperature (−1.90 °C). A time series during the final year of integration showed that net melting changed by a factor of 2–3 from July to October, with an annual average, relative to the Fox and Cooper (1994) ice shelf area, of 37 km^3/yr. However, the model resolution was insufficient to simulate melting near deep grounding lines where it is thought to be high (Rignot and Jacobs, 2002), and tides, which may be important for the transport of heat from the water to the ice shelf, were not included. But their result is within the range of our estimate. Assmann et al. (2003) used a coupled sea ice–ice shelf-ocean sigma coordinate model of the BRIOS (Bremerhaven Regional Sea Ice Ocean Simulations) family that crudely included the effect of tidal currents on the exchange of heat between water and the ice shelf by assuming a constant background current of the upper layer of water relative to the overlying ice shelf (Timmermann et al., 2002a). As with MICOM, ice shelf thickness was fixed and sub-ice water column data were taken from Greishar

and Bentley (1980). The model area extended from 50°S to 82°S as a circumpolar ring, thereby excluding the southernmost 20% of the cavity. NCEP reanalyses were used as surface forcing with ocean surface buoyancy fluxes provided by interaction with the coupled sea ice model. They found a pattern of basal melting and freezing similar to that of Holland et al. (2003), along with a strong seasonal cycle, but obtained a larger annual net melting of 85 km^3/yr over the portion of the ice shelf base assumed for our study. This is 40% higher than our upper limit for the average melt rate over the past 3 decades. These results provide no additional constraints on basal melting and little insight with respect to the different melt rates we obtain from salt and heat budget calculations.

5.4.4. Future work

This study and previous investigations reveal a large uncertainty in the basal melt rate beneath the Ross Ice Shelf. We show that salt and heat budgets for the ice cavity, with water through-flow calibrated using CFC data, differ by a factor of 3 in the basal melt rate. Estimates to date are dependant on either observations outside the ice cavity or results from circulation models that that do not adequately represent all of the processes and are not well constrained by data. There are tracers of glacial ice melt (O-18, neon, helium) that have not been utilized to their full potential, and analyses of these data in conjunction with hydrographic and CFC data should provide a better understanding of the net basal melting rate. Future observations should include this suite of tracers along with T, S and CFCs. Improvement of ocean circulation models with better forcing functions and mixing parameterizations, particularly for tidal mixing, and inclusion of anthropogenic and glacial melt tracers should also lead to a better understanding. Perhaps the most critical need is observations beneath the ice shelf, which are very expensive to acquire and are almost non-existent. Autonomous underwater vehicles may provide a cost-effective way of obtaining data in the future. Moorings fitted with temporal water sampling capability could provide useful velocity, thermohaline, and tracer observations at sites of known inflow and outflow. Satellite altimeters can directly measure changes in ice shelf elevation, and the distribution of basal melting and freezing assuming equilibrium conditions. However, some ice shelves appear to be thinning over the past decade, possibly due to changes in the basal melt rate. This has not been documented for the Ross Ice Shelf, but would have implications for the ocean properties and circulation that could be assessed with finely tuned numerical models and longer, better-targeted time series measurements.

6. Summary and conclusions

CTD/rosette stations with CFC measurements along the front of the Ross Ice Shelf in the austral summers of 1984, 1994 and 2000 showed rising CFC concentrations driven by the increases in the atmosphere, and decreasing salinities following a regional freshening trend since the 1960s. Water mass distributions remained similar over time with low and high-salinity shelf waters (LSSW + HSSW) to the east and west of the primary Ice Shelf Water (ISW) outflow plume near 180° longitude. ISW is colder than the sea surface freezing point because of subsurface ice shelf melting and has lower CFC concentrations because of its isolation from the atmosphere beneath the ice shelf. Modified Circumpolar Deep Water (MCDW) also has a relatively low CFC content due to its deep water component.

CFC concentrations (CFC-11, CFC-12, CFC-113) in HSSW and surface water were modeled using a time-dependent box model that included gas exchange with the atmosphere and inflow of MCDW onto the shelf. The modeled and observed CFC concentrations show the surface water to be undersaturated with respect to the atmosphere because sea ice retards gas exchange and a deepening mixed layer entrains low CFC MCDW. The average residence time of HSSW on the continental shelf over roughly the last 3 decades was modeled to range from 3.5 to 8 years but the conversion rate to ISW (see below) plus its direct flow off the shelf to the deep ocean favors the lower end of this range. HSSW CFC concentrations were used as the boundary condition to estimate the formation rate of ISW beneath the

western and central portion of the Ross Ice Shelf, with time-dependent box and stream tube models. These models gave formation (or outflow) rates of 0.88 and 0.84 Sv respectively, with the box model giving a sub-ice shelf residence time of ~3.5 years.

The freshening of HSSW during its conversion to ISW under the ice shelf yielded average net melt rates of 57 and 60 km^3/yr, whereas the rate calculated from the cooling of HSSW yielded only 20 km^3/yr. While these values may be taken as upper and lower limits over approximately three-fourths of the ice shelf base, the large discrepancy remains to be resolved. Possible reasons include mixing between LSSW and HSSW beneath the ice shelf prior to basal melting, mixing between lower and higher salinity varieties of ISW which form from LSSW and HSSW, and flow of meltwater across the grounding line which does not extract heat from seawater underlying the ice shelf. Oxygen isotopes and noble gas concentrations are strongly affected by glacial meltwater and may provide insight into the relative importance of the various processes that result in the formation of ISW. Work utilizing satellite radar measurements (e.g. Joughin and Padman, 2003) should also provide independent estimates of the distribution and volume of basal melting and freezing.

The ISW formation rates and basal melt rates presented here are from best fits of box and stream tube models to data taking during 1984, 1994 and 2000 cruises. However, model fits to individual data sets yield ISW formation rates and basal melt rates 3–4 times higher for the 1984 data set. We show that observed salinity variability on time scales shorter than times between our observations can cause variability in circulation time scales and apparent melt rates. However, the parallel salinity declines in HSSW and ISW suggest no persistent large changes occurred in the circulation or in the net basal melting rate under the Ross Ice Shelf over the past 3 decades.

Acknowledgements

We would like to thank H. Lee for performing the model calculations, E. Gorman, G. Mathieu and M. Mensch for measuring the CFC samples from the 1994 and 2000 cruises, S. Stammerjohn for extracting the sea ice concentrations for the NE Ross Sea from the NSIDC satellite data files, Patty Catanzaro for help in preparation of the figures, and Karen Assmann, David Holland, and three anonymous reviewers for helpful comments on the manuscript. This work was supported by cooperative agreements from the National Oceanographic and Atmospheric Administration (NOAA) through grants NA47GP0188 UCSIO PO 10075411, NA77RJ0453 UCSIO PO 10156283, and UCSIO PO 10196097-003 (CORC I, CORC II and ARCHES) to WMS and by NSF grant OPP02-33303 and the NASA Cryospheric Program to SSJ. The views expressed herein are those of the authors and do not necessarily reflect the views of NOAA or any of its sub-agencies. LDEO contribution number 6695.

References

Assmann, K., Hellmer, H.H., Beckmann, A., 2003. Seasonal variation in circulation and watermass distribution on the Ross Sea continental shelf. Antarctic Science 15 (1), 3–11.

Bentley, C.R., Jezek, K.C., 1981. RISS, RISP and RIGGS: post-IGY glaciological investigations of the Ross Ice Shelf in the US programme. Journal of Royal Society of New Zealand 11 (4), 355–372.

Bentley, C.R., Clough, J.W., Jezek, K.C., Shabtaie, S., 1979. Ice-thickness patterns and the dynamics of the Ross Ice Shelf, Antarctica. Journal of Glaciology 24 (90), 287–294.

Bergamasco, A., Defendi, V., Meloni, R., 2002. Some dynamics of water outflow from beneath the Ross Ice Shelf during 1995 and 1996. Antarctic Science 14 (1), 74–82.

Bullister, J.L., Weiss, R.F., 1988. Determination of CCl_3F and CCl_2F_2 in seawater and air. Deep-Sea Research 35, 839–853.

Busenberg, E., Plummer, L.N., 1992. Use of chlorofluorocarbons (CCl_3F and CCl_2F_2) as hydrologic tracers and age-dating tools: the alluvium and terrace system of central Oklahoma. Water Resources Research 28, 2257–2283.

Church, J.A., Gregory, J.M., Huybrechts, P., Kuhn, M., Lambeck, K., Nhuan, M.T., Qin, D., Woodworth, P.L., Anisimov, O.A., Bryan, F.O., Cazenave, A., Dixon, K.W., Fitzharris, B.B., Flato, G.M., Ganopolski, A., Gornitz, V., Lowe, J.A., Noda, A., Oberhuber, J.M., O'Farrell, S.P., Ohmura, A., Oppenheimer, M., Peltier, W.R., Raper, S.C.B., Ritz, C., Russell, G.L., Schlosser, E., Shum, C.K., Stocker, T.F., Stouffer, R.J., van de Wal, R.S.W., Voss, R., Wiebe, E.C., Wild, M., Wingham, D.J., Zwally, H.J., 2001.

Changes in Sea Level. Climate Change 2001. In: Houghton, J.T., et al. (Eds.), The Scientific Basis. WG1 TAR IPCC. Cambridge University Press, Cambridge, pp. 639–693.

Cunnold, D.M., Weiss, R.F., Prinn, R.G., Hartley, D., Simmonds, P.G., Fraser, P.J., Miller, B., Alyea, G.N., Porter, L., 1997. GAGE/AGAGE measurements indicating reductions in global emissions of CCl_3F and CCl_2F_2 in 1992–1994. Journal of Geophysical Research 102, 1259–1269.

Davey, F., 1995. Bathymetry, Plate 1, from ANTOSTRAT Project, Seismic Stratigraphic Atlas of the Ross Sea, Antarctica. In: A.R. Cooper, et al. (Eds.), Geology and Seismic Stratigraphy of the Antarctic Margin, Antarctic Research Series 68, Map 1a.

Dieckmann, G., Rohardt, G., Hellmer, H.H., Kipfstuhl, J., 1986. The occurrence of ice platelets at 250 m depth near the Filchner Ice Shelf and its significance for sea ice biology. Deep-Sea Research 33 (2), 141–148.

Elkins, J., Thompson, T., Swanson, T., Butler, J., Hall, B., Cummings, S., Fisher, D., Raffo, A., 1993. Decrease in the growth rates of atmospheric chlorofluorocarbons -11 and -12. Nature 364, 780–783.

Fox, A.J., Cooper, A.P.R., 1994. Measured properties of the Antarctic ice sheet derived from the SCAR Antarctic digital database. Polar Record 30 (174), 201–206.

Fricker, H.A., Popov, S., Allison, I., Young, N., 2001. Distribution of marine ice beneath the Amery Ice Shelf. Geophysical Research Letters 28 (11), 2241–2244.

Gade, H., 1979. Melting of ice in sea water: a primitive model with application to the Antarctic Ice Shelf and Icebergs. Journal of Physical Oceanography 9 (1), 189–198.

Greishar, L.L., Bentley, C.R., 1980. Isostatic equilibrium grounding line between the West Antarctic inland ice sheet and the Ross Ice Shelf. Nature 283, 651–654.

Grosfeld, K., Hellmer, H.H., Jonas, M., Sandhager, H., Schulte, M., Vaughan, D.G., 1998. Marine ice beneath Filchner Ice Shelf: evidence from a multi-disciplinary approach. Antarctic Research Series 75, 319–339.

Hellmer, H.H., 2004. Impact of Antarctic ice shelf basal melting on sea ice and deep ocean properties. Geophysical Research Letters 31, GL019506.

Hellmer, H.H., Jacobs, S.S., 1995. Seasonal circulation under the eastern Ross Ice Shelf, Antarctica. Journal Geophysical Research 100 (C6), 10873–10885.

Hellmer, H.H., Jacobs, S.S., Jenkins, A., 1998. Oceanic erosion of a floating Antarctic glacier in the Amundsen Sea. Antarctic Research Series 75, 83–99.

Hohmann, R., Schlosser, P., Jacobs, S.S., Ludin, A., Weppernig, R., 2002. Excess helium and neon in the Southeast Pacific: tracers for glacial meltwater. Journal of Geophysical Research 107 (C11), 3198 JC000378.

Holland, D.M., Jacobs, S.S., Jenkins, A., 2003. Modeling the ocean circulation beneath the Ross Ice Shelf. Antarctic Science 15 (1), 13–23.

Jacobs, S.S., Comiso, J.C., 1989. Sea ice and oceanographic processes on the Ross Sea continental shelf. Journal of Geophysical Research 94, 18195–18211.

Jacobs, S.S., Giulivi, C.F., 1998. Interannual ocean and sea ice variability in the Ross Sea. Antarctic Research Series 75, 135–150.

Jacobs, S.S., Amos, A.F., Bruchhausen, P.M., 1970. Ross Sea oceanography and Antarctic bottom water formation. Deep-Sea Research 17, 935–962.

Jacobs, S.S., Gordon, A.L., Ardai, J.L., 1979. Circulation and melting beneath the Ross Ice Shelf. Science 203, 439–442.

Jacobs, S.S., Fairbanks, R.G., Horibe, Y., 1985. Origin and evolution of water masses near the Antarctic continental margin: evidence from $H_2^{18}O/H_2^{16}O$ ratios. Antarctic Research Series 43, 59–85.

Jacobs, S.S., Hellmer, H.H., Doake, C.S.M., Jenkins, A., Frolich, R., 1992. Melting of ice shelves and the mass balance of Antarctica. Journal of Glaciology 130, 375–387.

Jacobs, S.S., Giulivi, C.F., Mele, P.A., 2002. Freshening of the Ross Sea during the late 20th Century. Science 297, 386–389.

Jenkins, A., Bombosch, A., 1995. Modeling the effects of frazil ice crystals on the dynamics and thermodynamics of ice shelf water plumes. Journal of Geophysical Research 100 (C4), 6967–6981.

Jenkins, A., Vaughan, D.G., Jacobs, S.S., Hellmer, H.H., Keys, J.R., 1997. Glaciological and oceanographic evidence of high melt rates beneath Pine Island Glacier, West Antarctica. Journal of Glaciology 43 (143), 114–121.

Joughin, I., Padman, L., 2003. Melting and freezing beneath Filchner–Ronne Ice Shelf, Antarctica. Geophysical Research Letters 30 (9), 1477.

Killworth, P.D., 1974. A baroclinic model of motions on Antarctic continental shelves. Deep-Sea Research 21 (10), 815–838.

Kurtz, D.D., Bromwich, D.H., 1985. A recurring, atmospherically forced polynya in Terra Nova Bay. Antarctic Research Series 43, 177–201.

Lingle, C.S., Schilling, D.H., Fastook, J.L., Paterson, W.S.B., Brown, T.J., 1991. A flow band model of the Ross Ice Shelf, Antarctica: response to CO_2-induced climatic warming. Journal of Geophysical Research 96 (B4), 6849–6871.

MacAyeal, D.R., 1984. Thermohaline circulation below the Ross Ice Shelf: a consequence of tidally induced vertical mixing and basal melting. Journal of Geophysical Research 89 (C1), 597–606.

MacAyeal, D.R., 1985. Evolution of tidally triggered meltwater plumes below ice shelves. Antarctic Research Series 43, 133–143.

Mensch, M., Bayer, R., Bullister, J.L., Schlosser, P., Weiss, R.F., 1996. The distribution of tritium and CFCs in the Weddell Sea during the mid-1980s. Progress in Oceanography 38, 377–415.

Mensch, M., Smethie Jr., W.M., Schlosser, P., Weppernig, R., Bayer, R., 1998. Transient tracer distributions observed during the drift and recovery of Ice Station Weddell, ocean, ice and atmosphere: interactions at the Antarctic continental margin. Antarctic Research Series 75, 241–256.

NCEP, 2002. http://ingrid.ldeo.columbia.edu/SOURCES/.NOAA/.NCEP-NCAR/.CDAS-1/.MONTHLY/.

Neal, C.S., 1979. The dynamics of the Ross Ice Shelf revealed by radio echo-sounding. Journal of Glaciology 24 (90), 295–307.

Nicholls, K.W., Makinson, K., 1998. Ocean circulation beneath the western Ronne Ice Shelf as derived from in situ measurements of water currents and properties. Antarctic Research Series 75, 301–318.

Nicholls, K.W., Osterhus, S., Makinson, K., Johnson, M.R., 2001. Oceanographic conditions south of Berkner Island, beneath the Filchner–Ronne Ice Shelf, Antarctica. Journal of Geophysical Research 106 (C6), 11481–11492.

Nost, O.A., Foldvik, A., 1994. A model of ice shelf-ocean interaction with application to the Filchner–Ronne and Ross Ice Shelves. Journal of Geophysical Research 99 (C7), 14243–14254.

Orsi, A.H., Smethie Jr., W.M., Bullister, J.L., 2002. On the total input of Antarctic waters to the deep ocean: a preliminary estimate from chlorofluorocarbon measurements. Journal of Geophysical Research 107 (C8) 31-1–31-14.

Padman, L., Erofeeva, S., Joughin, I., 2003. Tides of the Ross Sea and Ross Ice Shelf cavity. Antarctic Science 15 (1), 31–40.

Pillsbury, R.D., Jacobs, S.S., 1985. Preliminary observations from long-term current meter moorings near the Ross Ice Shelf, Antarctica. Antarctic Research Series 43, 87–107.

Rignot, E., Jacobs, S.S., 2002. Rapid bottom melting widespread near Antarctic Ice Sheet grounding lines. Science 296, 2020–2023.

Robertson, R., Visbeck, M., Gordon, A.L., Fahrbach, E., 2002. Long-term temperature trends in the deep waters of the Weddell Sea. Deep-Sea Research II 49, 4791–4806.

Robertson, R., Beckmann, A., Hellmer, H., 2003. M_2 tidal dynamics in the Ross Sea. Antarctic Science 15 (1), 41–46.

Scheduikat, M., Olbers, D.J., 1990. A one-dimensional mixed layer model beneath the Ross Ice Shelf with tidally induced vertical mixing. Antarctic Science 2 (1), 29–42.

Schlosser, P., Bayer, R., Foldvik, A., Gammelsrod, T., Rohardt, G., Munnich, K.O., 1990. Oxygen 18 and helium as tracers of ice shelf water/ice interaction in the Weddell Sea. Journal of Geophysical Research 95 (C3), 3253–3263.

Schlosser, P., Collon, P., Winckler, G., Newton, R., Jacobs, S., 2003. Glacial meltwater fractions in the Ice Shelf Water derived from stable isotopes and noble gases: comparison of the Filchner Ronne and Ross Ice Shelves. EOS Transactions, American Geophysical Union 84 (46), F388.

Shabtaie, S., Bentley, C.R., 1987. West Antarctic ice streams draining into the Ross Ice Shelf: configuration and mass balance. Journal of Geophysical Research 92 (B2), 1311–1336.

Smethie Jr., W.M., Schlosser, P., Hopkins, T.S., Boenisch, G., 2000. Renewal and circulation of intermediate waters in the Canadian Basin observed on the SCICEX-96 cruise. Journal of Geophysical Research 105, 1105–1121.

Timmermann, R., Hellmer, H.H., Beckmann, A., 2002a. Simulations of ice-ocean dynamics in the Weddell Sea 1. Model configuration and validation. Journal of Geophysical Research 107 1029/2000JC000741.

Timmermann, R., Hellmer, H.H., Beckmann, A., 2002b. Simulations of ice-ocean dynamics in the Weddell Sea 2. Interannual variability 1985–1993. Journal of Geophysical Research 107 1029/2000JC000742.

Trumbore, S.E., Jacobs, S.S., Smethie, W.M., 1991. Chlorofluorocarbon evidence for rapid ventilation of the Ross Sea. Deep-Sea Research 38 (7), 845–870.

Walker, S.J., Weiss, R.F., Salameh, P.K., 2000. Reconstructed histories of annual mean atmospheric mole fractions for the halocarbons CFC-11, CFC-12, CFC-113 and carbon tetrachloride. Journal of Geophysical Research 105, 14285–14296.

Wanninkhof, R., 1992. Relationship between wind speed and gas exchange over the ocean. Journal of Geophysical Research 97, 7373–7382.

Weiss, R.F., Ostlund, H.G., Craig, H., 1979. Geochemical studies of the Weddell Sea. Deep-Sea Research 26A, 1093–1120.

Willey, D.A., Fine, R.A., Sonnerup, R.E., Bullister, J.L., Smethie Jr., W.M., Warner, M.J., 2004. Global ocean chlorofluorocarbon inventory. Geophysical Research Letters 31, L01303.

Williams, M.J.M., Jenkins, A., Determann, J., 1998. Physical controls on ocean circulation beneath ice shelves revealed by numerical models. Antarctic Research Series 75, 285–299.

Zotikov, I.A., Zagarodnov, V.S., Raikovsky, J.V., 1980. Core drilling through the Ross Ice Shelf (Antarctica) confirmed basal freezing. Science 207, 1463–1465.

Zwally, H.J., Comiso, J.C., Gordon, A.L., 1985. Antarctic offshore leads and polynyas and oceanographic effects. Antarctic Research Series 43, 203–226.